A-year Continuous Observations of Near-Surface Atmospheric Water Vapor Stable Isotopes at Matara, Sri Lanka

Yuqing Wu [1, 2], Jing Gao [1, 3, *], Aibin Zhao [1], Xiaowei Niu [1], Yigang Liu [1, 2], Disna Ratnasekera [4, 5], Tilak Priyadarshana Gamage [6], Amarasinghe Hewage Ruwan Samantha [6]

1 State Key Laboratory of Tibetan Plateau Earth System, Resources and Environment, Institute of Tibetan Plateau Research, Chinese Academy of Sciences, Beijing 100101, China

2 University of Chinese Academy of Sciences, Beijing, 100049, China

3 Lanzhou University, Lanzhou 733000, China

4 China-Sri Lanka Joint Center for Education & Research, Guangzhou 510301, China

5 Department of Agricultural Biology, Faculty of Agriculture, University of Ruhuna, Matara 81000, Sri Lanka

6 Faculty of Fisheries and Marine Sciences & Technology, University of Ruhuna, Matara 81000, Sri Lanka

* *Corresponding to*: Jing Gao (gaojing@itpcas.ac.cn)

Text S1 Calibration of the water vapor isotopic analyzer

Measurements of water vapor isotopic composition by the Los Gatos Research (LGR) analyzer are not used directedly but the instrument needs to be the calibrated as the measurements are affected by internal and external conditions of the LGR analyzer, hence the measured values of cannot simply be corrected with standard samples. The following factors can affect measurement accuracy: concentration changes, instrumental effects, and drift effects (Benetti et al., 2014; Johnson et al., 2011). Measurements of water vapor stable isotope values become inconsistent when measured under different water vapor concentrations. The result is correlated to water vapor concentration (either linearly or non-linearly), which is the so-called concentration-dependent effect (Steen-Larsen et al., 2013). In addition, minor variations in the inherent characteristics of each stable isotope analyzer led to disparities between measured and "true" isotope values, a phenomenon referred to as instrumental effect. When an analyzer is in continuous operation, optical components experience aging, including a reduction in the reflectivity of cavity mirrors. These factors collectively contribute to instrument drift (Bailey et al., 2015; Rambo et al., 2011).

As the magnitude of these drift effects vary between analyzers, it is crucial to evaluate and correct these errors using standard samples. In our study, we followed the calibration protocol from Steen-Larsen et al. (2013).

Text S1.1 Humidity correction

The humidity measurements obtained from the LGR analyzer (absolute humidity in ppmv) are compared to humidity values calculated from the automated weather

station (AWS) measurements (calculated from relative humidity and temperature) in Fig. S1. The best linear fit is given by a function:

$$y = (1.03\pm0.003)\ x + (-288.67\pm41.46)\ (r = 0.97, n = 6349) \quad \text{(S1)}$$

where x is the LGR and y is the AWS humidity values (in ppmv), respectively. Equation (S1) is hereafter used to convert all LGR humidity data into the meteorological instrument scale.

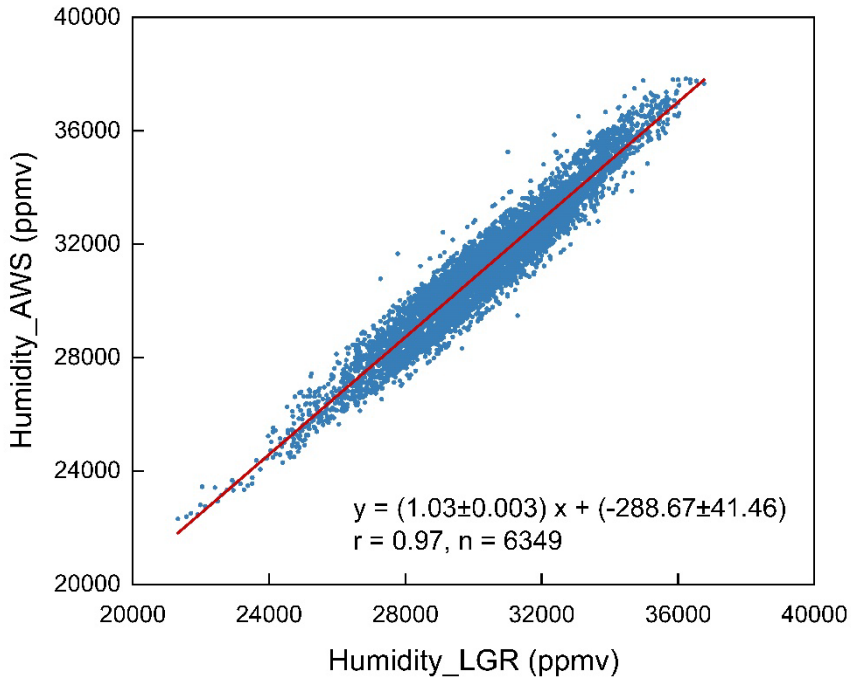

Figure S1: Humidity measurements: Meteorological sensor vs. LGR measurements. The red line represents the linear fit.

Text S1.2 Humidity-isotope response calibration

A memory effect manifests when standard samples of differing concentrations are being tested in the host system's testing chamber as remnants of a previous sample may remain in the testing chamber and introduce a discernible contamination of measurements of subsequent samples. During standard sample testing, we performed a 25- or 30-minute test for each gradient. While filtering the measured isotope standard

sample data, the initial 10 or 15 minutes and the last 30 seconds of each standard sample segment were eliminated.

When conducting field observations, whether on a daily or seasonal basis, there is always a substantial fluctuation in water vapor concentrations. The errors resulting from concentration effects are incomparable to other factors. In our measurements, concentration calibration was performed monthly.

Based on previous research (Steen-Larsen et al., 2013; Steen-Larsen et al., 2015; Ritter et al., 2016), we chose 20,000 ppmv as the reference water vapor concentration, based on the assumption that isotope concentration effects are minimal under this standard. Our objective was to calculate the stable isotope mean values at this reference concentration. Given the generally high values of water vapor concentration at Matara station, we conducted the measurement of isotopic values for standard samples at a range of water vapor concentration from 16,000 to 38,000 ppmv using increments of 1,000 ppmv. We excluded measurements with average H_2O below 13,000 ppmv or higher 40,000 ppmv and standard deviations of H_2O, $\delta^{18}O$, and δD (denoted as Δ (H_2O), Δ ($\delta^{18}O$), Δ (δD), respectively) higher than 200 ppmv, 0.2‰, and 1‰, respectively. Subsequently, we calculated the disparities between the average isotopic values at 20,000 ppmv water vapor concentration and the measurements of standard samples under various concentration gradients to establish a nonlinear relationship between isotope values and water vapor concentration (Fig. S2). It has been proven that polynomial functions yield the most effective fit to LGR analyzer data. The fit curve equations for hydrogen and oxygen stable isotope data, as well as for water vapor

77 concentration, were then applied to correct the concentrations obtained from actual
78 measurements of atmospheric water vapor.

79 The calculation to correct for concentration effects can be expressed using the
80 following formula:

$$\delta_{\text{Humidity correction vs. reference level}} = \delta_{\text{Humidity-isotope response}}\left(c(H_2{}^{16}O_{\text{ppmv}})\right) \quad \text{(S2)}$$

$$\delta_{\text{Measured humidity-correction to reference level}} = \delta_{\text{Measured}} - \delta_{\text{Humidity correction vs. reference level}} \quad \text{(S3)}$$

81 where δ_{Measured} represents the raw measurement and $\delta_{\text{Humidity-isotope response}}$ is the humidity-
82 isotope response function defining the difference between the measured and true
83 isotopic composition for a reference (20,000 ppmv) vapor introduced at different
84 humidity levels.

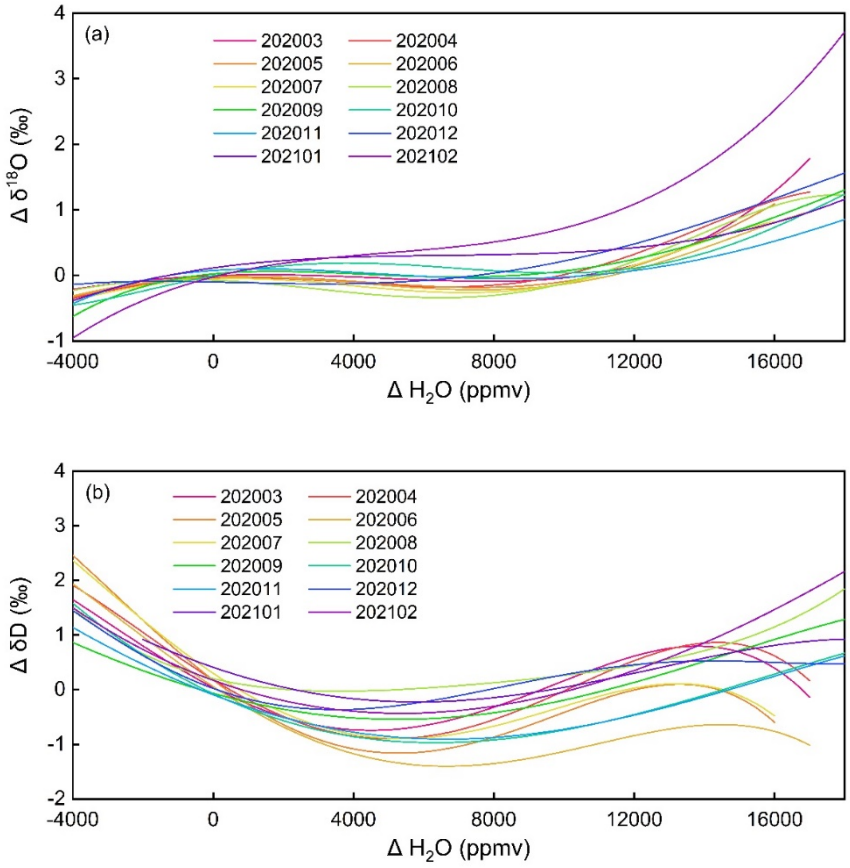

Figure S2: Water vapor concentration dependent correction curves between Δ (H_2O) and (a) Δ ($\delta^{18}O$) and (b) Δ (δD) for the standard samples at Matara station, covering the period from March 2020 to February 2021. Different colors identify different months (using the yyyymm notation).

Text S1.3 Known-standard calibration

Each LGR analyzer has its own unique characteristics, which lead to differences between measured and actual isotope values. To correct these measurements errors caused by instrument bias, it is imperative to create a conversion function connecting instrument results ($\delta^{18}O$ and δD) with the Vienna Standard Mean Ocean Water - Standard Light Antarctic Precipitation (VSMOW-SLAP) standard. It is essential to have a minimum of two or more standard samples with known isotope compositions to

establish a linear functional relationship. The formula for the linear relationship used in the VSMOW-SLAP calibration is as follows:

$$\frac{\delta_{st2\_true} - \delta_{st1\_true}}{\delta_{st2\_mean\_ref} - \delta_{st1\_mean\_ref}} = \frac{\delta_{humidity\_VSMOW\_correction} - \delta_{st1\_true}}{\delta_{humidity\_correction} - \delta_{st1\_mean\_ref}} \quad (S4)$$

$$\delta_{humidity\_VSMOW\_correction} = \frac{(\delta_{st2\_true} - \delta_{st1\_true}) * (\delta_{humidity\_correction} - \delta_{st1\_mean\_ref})}{\delta_{st2\_mean\_ref} - \delta_{st1\_mean\_ref}} + \delta_{st1\_true} \quad (S5)$$

δ_{st1_true} and δ_{st2_true} are the true values of standards st1 and st2. $\delta_{st1\_mean\_ref}$ and $\delta_{st2\_mean\_ref}$ is the measured values of standards st1 and st2, which have been humidity corrected to a reference level following formulas (S2) and (S3).

Two standard samples were tested at different concentration gradients (ranging from 16,000 to 38,000 with increments of 1,000) for either 25 or 30 minutes on the same day each month. When inspecting and screening the test data, we manually eliminated potential data anomalies to ensure that the standard deviations for H_2O, $\delta^{18}O$, and δD of valid data within each concentration gradient remained below 200 ppmv, 0.2‰, and 1‰, respectively.

Text S1.4. Drift correction

The double-inlet mode of the LGR analyzer allows alternate measurements of ambient water vapor and reference water, effectively correcting for the assumed linear drift between measurements and reference waters. Measurements were taken using 12-hour intervals, and concentration-dependent calibration and instrumental bias correction were performed daily. Drift is corrected using the following equation:

$$\delta_{\text{drift corrected VSMOW}} = \delta_{\text{st1\_t1}} \times T + \delta_{\text{st1\_t2}} \times (1 - T) - \delta_{\text{st1\_true}} \quad \text{(S6)}$$

$$\delta_{\text{measured VSMOW drift corrected}} = \delta_{\text{measured VSMOW}} - \delta_{\text{drift corrected VSMOW}} \quad \text{(S7)}$$

where $T=\frac{t-t_1}{t_2-t_1}$, and t_1 and t_2 are the respective times when δ_{st1_t1} and δ_{st1_t2} were measured for the water vapor standard samples. δ_{st1_true} is the true value of the water used to produce the vapor stream.

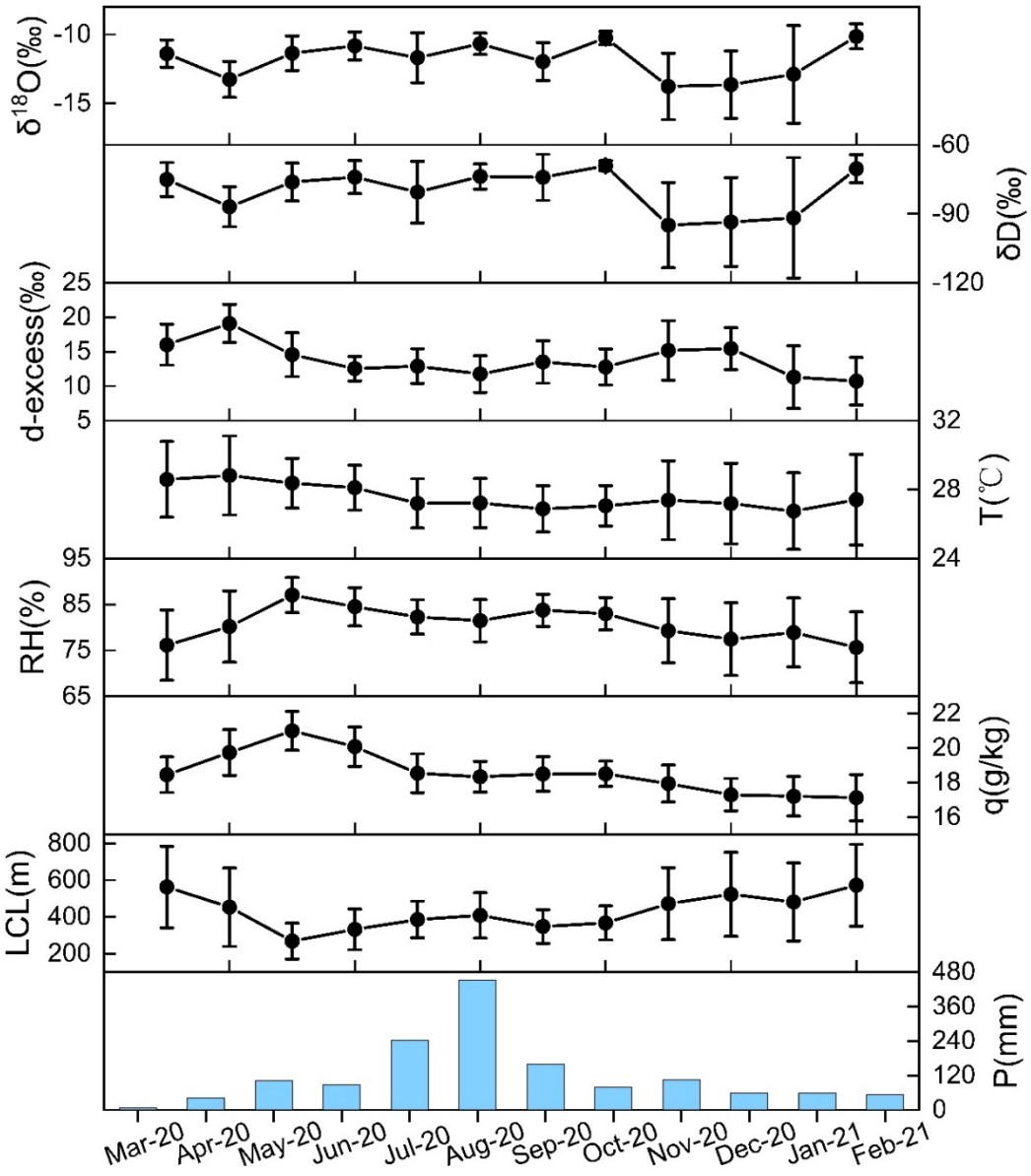

Figure S3: Temporal Evolution of Monthly Averages

This figure presents the temporal evolution of monthly averages of atmospheric water vapor stable isotopes ($\delta^{18}O$, δD, d-excess) alongside co-occurring meteorological parameters such as temperature (T), relative humidity (RH), specific humidity (q), lifting condensation level (LCL), and precipitation (P).

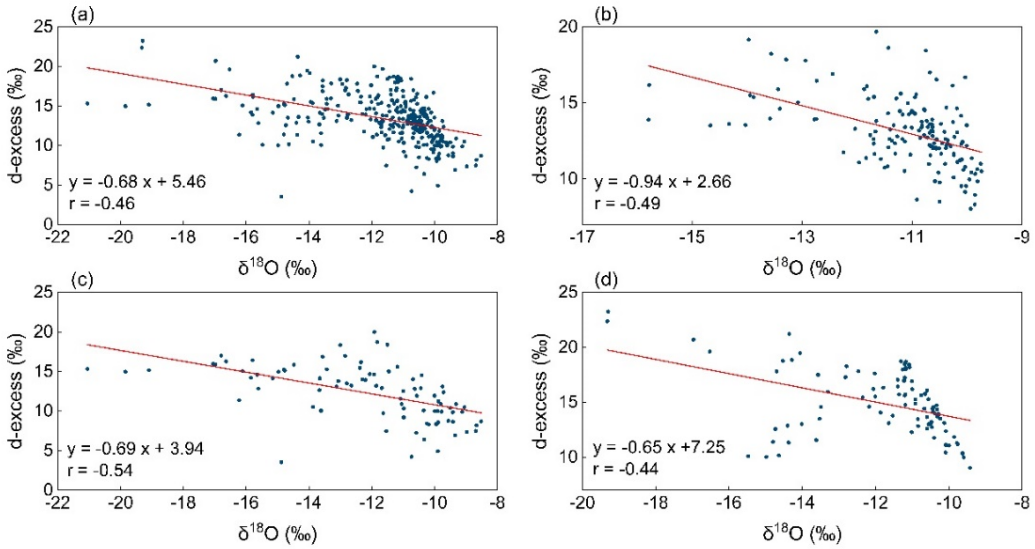

Figure S4: Co-variations of Water Vapor Isotopic Composition and d-excess

These subfigures display the co-variations of water vapor $\delta^{18}O$ and d-excess during the different periods, including the complete period, southwest monsoon, northeast monsoon, and non-monsoon seasons. Red lines indicate the least squares linear regression, highlighting trends in the data.

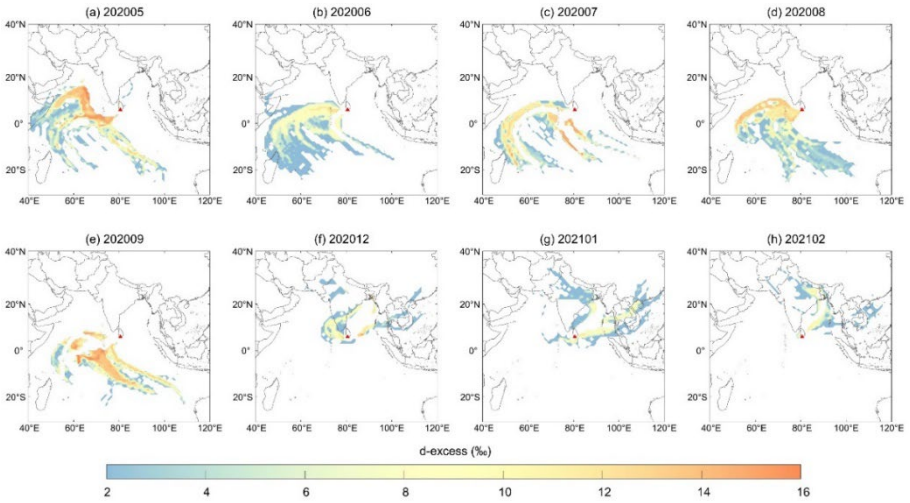

130

131 **Figure S5: Monthly Concentration Fields of d-excess for 168h HYSPLIT Back**

132 **Trajectories**

133 These figures show the spatial distribution of d-excess for 168-hour HYSPLIT

134 back trajectories during the southwest monsoon and the northeast monsoon. The red

135 triangle marks the study site, while the yellow solid line boxes highlight specific regions

136 of moisture sources during the two monsoon periods.

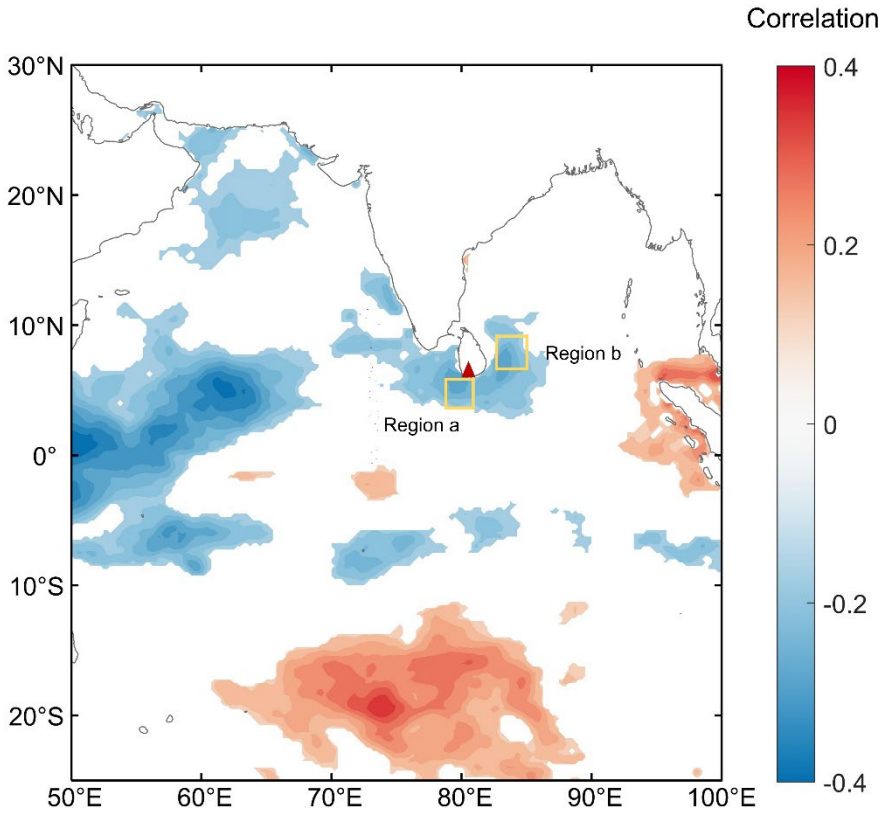

Figure S6: Spatial Distribution of Correlation between Water Vapor d-excess and RH_{SST}

This figure illustrates the spatial distribution of the correlation between water vapor d-excess observed at the Matara station and RH_{SST} (calculated relative to the saturation vapor pressure at sea surface temperature) in the surrounding sea area during the observation period. The solid red triangle denotes the location of the Matara station.

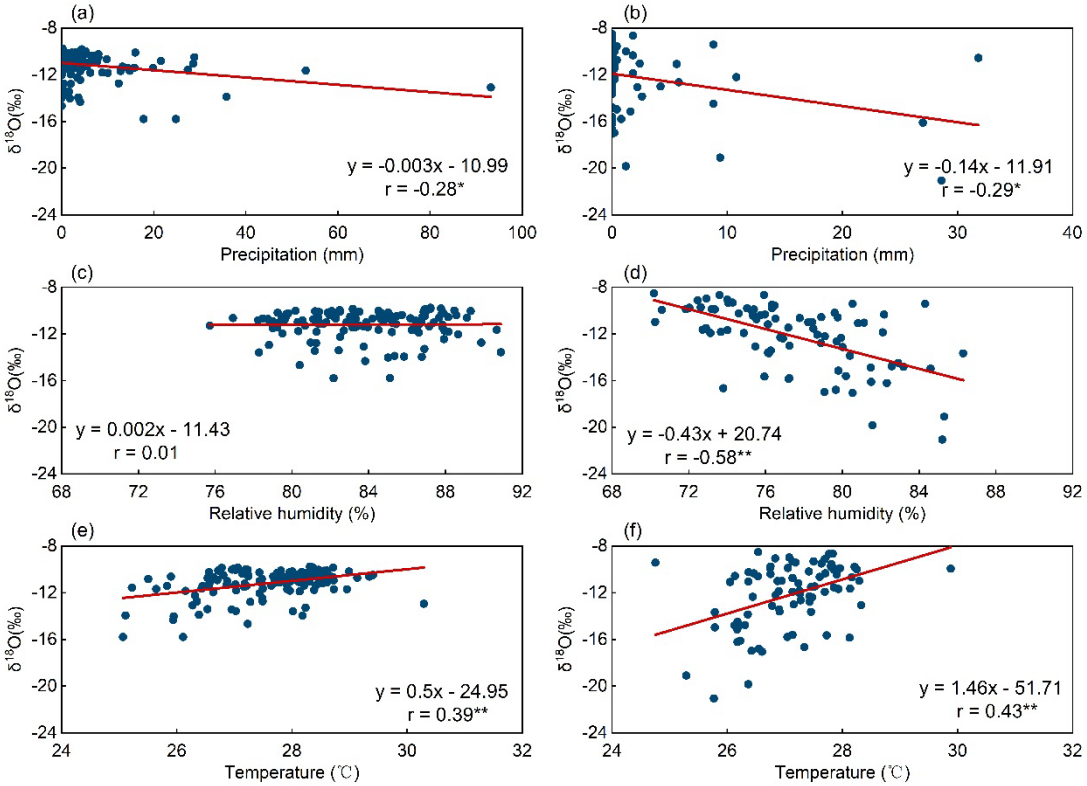

144

145 **Figure S7: Correlation Analysis of Meteorological Parameters and Water Vapor**

146 **Isotopic Composition**

147 These subfigures present the results of correlation analyses of $\delta^{18}O$ with

148 precipitation amount, relative humidity, and 2m air temperature during the southwest

149 monsoon and the northeast monsoon. The number of r represents the correlation

150 coefficient (** and * indicate that the correlation coefficients passed the t-test of 0.01

151 and 0.05 significant level, respectively).

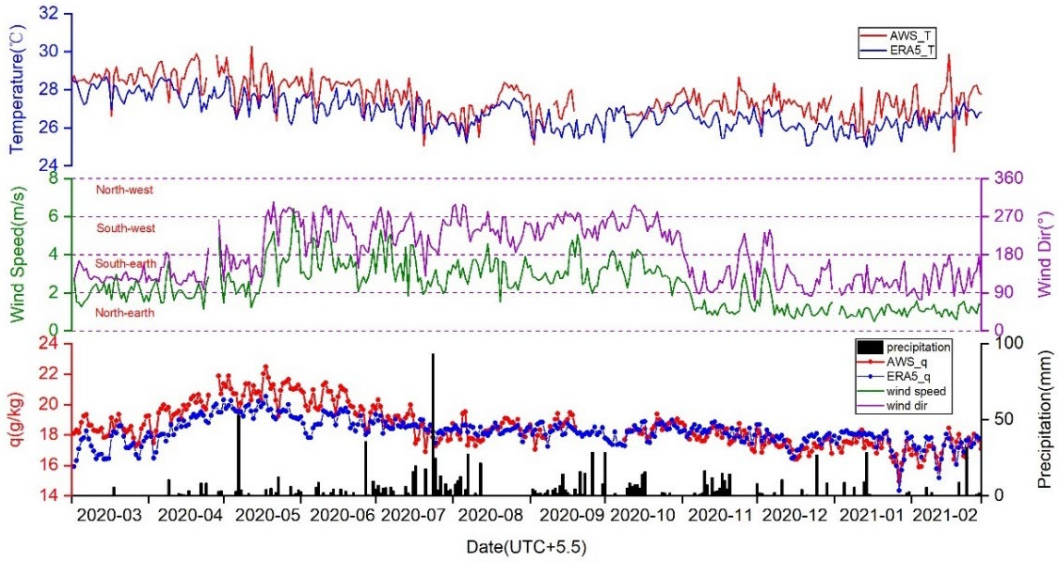

Figure S8: Time Series of Meteorological Parameters

This figure shows the time series of temperature (T), specific humidity (q), wind speed, wind direction, and daily precipitation observed by AWS (Automated Weather Station), as well as simulated temperature and specific humidity from ERA5.

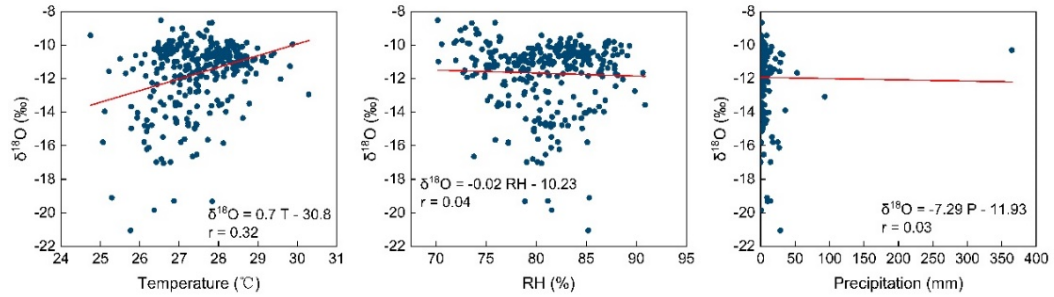

Figure S9: Co-variations of Water Vapor Isotopic Composition and Meteorological Parameters

These subfigures depict the co-variations of water vapor isotopic composition with meteorological parameters such as temperature (T), relative humidity (RH), and precipitation. Red lines represent the least squares linear regression, providing insights into the relationships between isotopic composition and meteorological variables.

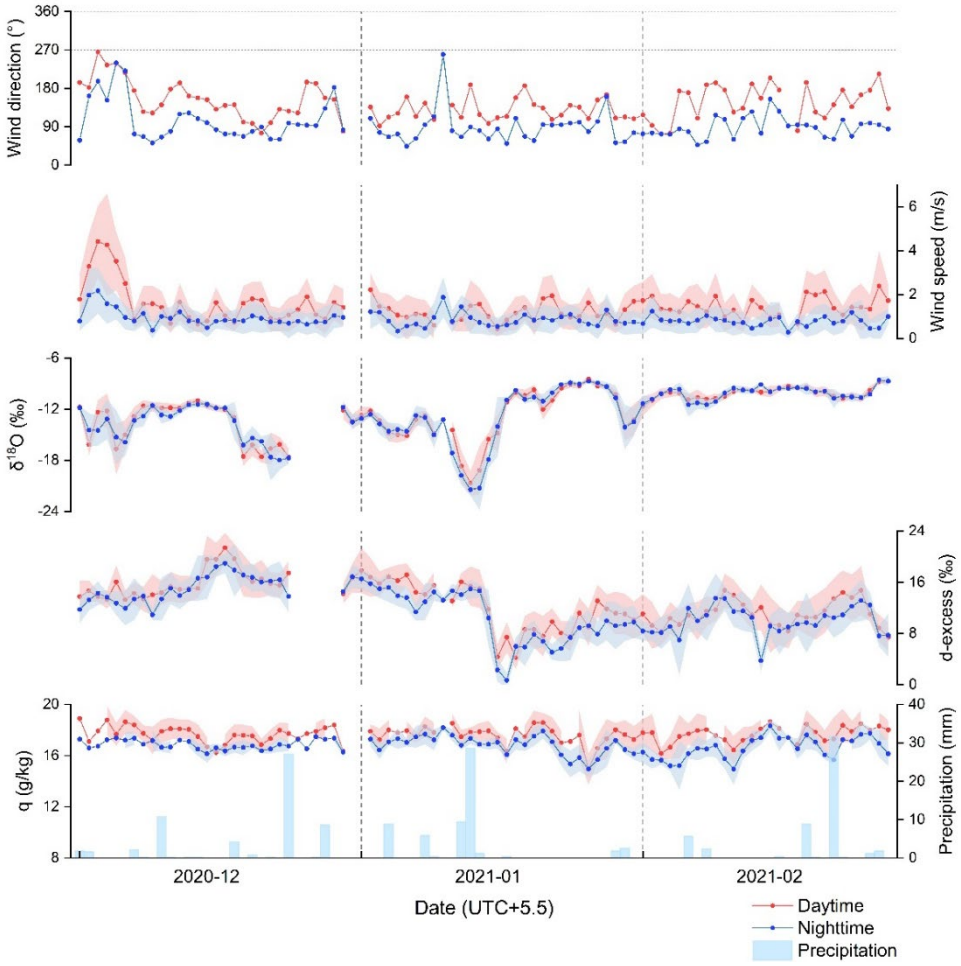

Figure S10: Time Series of Daily Precipitation, Isotopic Composition, and Meteorological Parameters during the Northeast Monsoon

This figure displays the time series of daily precipitation, isotopic composition ($\delta^{18}O$, d-excess), specific humidity (q), wind speed, and wind direction during the northeast monsoon using 12-hour sampling intervals (day-night). Red and blue dotted lines represent the daytime and nighttime measurements, respectively, offering a comprehensive view of diurnal variations.

Table S1: Abbreviations of variable names used in this paper.

Variable name	Physical meaning	Unit
ENSO	El Niño-Southern Oscillation	
ITCZ	Intertropical Convergence Zone	
AS	Arabian Sea	
BoB	Bay of Bengal	
GNIP	Global Network of Isotopes in Precipitation	
ISM	Indian Summer Monsoon	
VSMOW	Vienna Standard Mean Ocean Water	
AWS	Automated weather station	
BLH	Atmospheric boundary layer height	m
OLR	Outgoing longwave radiation	W/m^2
HYSPLIT	Hybrid Single-Particle Lagrangian Integrated Trajectory	
NOAA	National Oceanic and Atmospheric Administration	
GDAS	Global Data Assimilation System	
CWT	Concentration-weighted trajectory	
T	Temperature	℃
q	Specific humidity	g/kg
P	Precipitation	mm
RH	Relative humidity	%
SST	Sea surface temperature	℃
RH_{SST}	Relative humidity of the sea-surface air	%
LCL	Lifting condensation level	m
SD	Standard deviation	
LMWL	Local Meteoric Water Line	
GMWL	Global Meteoric Water Line	

175

References

Bailey, A., Noone, D., Berkelhammer, M., Steen-Larsen, H.C., and Sato, P.: The stability and calibration of water vapor isotope ratio measurements during long-term deployments, Atmos. Meas. Tech., 8, 4521-4538, https://doi.org/10.5194/amt-8-4521-2015, 2015.

Benetti, M., Reverfdin, G., Pierre, C., Merlivat, L., Risi, C., Steen-Larsen, H.C., and Vimeux, F.: Deuterium excess in marine water vapor: Dependency on relative humidity and surface wind speed during evaporation, J. Geophys. Res. Atmos., 119, 584-593, https://doi.org/10.1002/2013JD020535, 2014.

Johnson, L.R., Sharp, Z.D., Galewsky, J., Strong, M., Van Pelt, A.D., Dong, F., and Noone, D.: Hydrogen isotope correction for laser instrument measurement bias at low water vapor concentration using conventional isotope analyses: application to measurements from Mauna Loa Observatory, Hawaii, Rapid Commun. Mass Sp., 25, 608-616, https://doi.org/10.1002/rcm.4894, 2011.

Rambo, J., Lai, C-T., Farlin, J., Schroeder, M., and Bible, K.: On-Site Calibration for High Precision Measurements of Water Vapor Isotope Ratios Using Off-Axis Cavity-Enhanced Absorption Spectroscopy, J. Atmos. Ocean. Tech., 28, 1448-1457, https://doi.org/10.1175/JTECH-D-11-00053.1, 2011.

Ritter, F., Steen-Larsen, H.C., Werner, M., Masson-Delmotte, V., Orsi, A., Behrens, M., Birnbaum, G., Freitag, J., Risi, C., and Kipfstuhl, S.: Isotopic exchange on the diurnal scale between near-surface snow and lower atmospheric water vapor at Kohnen station, East Antarctica, J. Geophys. Res., 10, 1-35,

https://doi.org/10.5194/tc-2016-4, 2016.

Steen-Larsen, H.C., Johnsen, S.J., Masson-Delmotte, V., Stenni, B., Risi, C., Sodemann, H., Balslev-Clausen, D., Blunier, T., Dahl-Jensen, D., Ellehøj, M.D., Falourd, S., Grindsted, A., Gkinis, V., Jouzel, J., Popp, T., Sheldon, S., Simonsen, S.B., Sjolte, J., Steffensen, J.P., Sperlich, P., Sveinbjörnsdóttir, A.E., Vinther, B.M., and White, J.W.C.: Continuous monitoring of summer surface water vapor isotopic composition above the Greenland Ice Sheet, Atmos. Chem. Phys., 13, 4815-4828, https://doi.org/10.5194/acp-13-4815-2013, 2013.

Steen-Larsen, H.C., Sveinbjörnsdottir, A.E., Jonsson, T., Ritter, F., Bonne, J-L., Masson-Delmotte, V., Sodemann, H., Blunier, T., Dahl-Jensen, D., and Vinther, B.M.: Moisture sources and synoptic to seasonal variability of North Atlantic water vapor isotopic composition, J. Geophys. Res. Atmos., 120, 5757-5774, https://doi.org/10.1002/2015JD023234, 2015.